NASA TECHNICAL NOTE

NASA TN D-7098

NASA TN D-7098

A COMPARISON OF TECHNIQUES FOR INVERSION OF RADIO-RAY PHASE DATA IN PRESENCE OF RAY BENDING

by H. Andrew Wallio and Mario D. Grossi

Langley Research Center
Hampton, Va. 23365

NATIONAL AERONAUTICS AND SPACE ADMINISTRATION • WASHINGTON, D. C. • NOVEMBER 1972

1. Report No.	2. Government Accession No.	3. Recipient's Catalog No.
NASA TN D-7098		

4. Title and Subtitle	5. Report Date
A COMPARISON OF TECHNIQUES FOR INVERSION OF RADIO-RAY PHASE DATA IN PRESENCE OF RAY BENDING	November 1972
	6. Performing Organization Code

7. Author(s)	8. Performing Organization Report No.
H. Andrew Wallio, Langley Research Center; and Mario D. Grossi, Raytheon Company	L-8275
	10. Work Unit No. 815-20-04-23-02
9. Performing Organization Name and Address	11. Contract or Grant No.
NASA Langley Research Center Hampton, Va. 23365	
	13. Type of Report and Period Covered
12. Sponsoring Agency Name and Address	Technical Note
National Aeronautics and Space Administration Washington, D.C. 20546	14. Sponsoring Agency Code

15. Supplementary Notes

16. Abstract

Derivations are presented of the straight-line Abel transform and the seismological Herglotz-Wiechert transform (which takes into account ray bending) that are used in the reconstruction of refractivity profiles from radio-wave phase data. Profile inversion utilizing these approaches, performed in computer-simulated experiments, are compared for cases of positive, zero, and negative ray bending. For thin atmospheres and ionospheres, such as the Martian atmosphere and ionosphere, radio-wave signals are shown to be inverted accurately with both methods. For dense media, such as the solar corona or the lower Venus atmosphere, the refractivities recovered by the seismological Herglotz-Wiechert transform provide a significant improvement compared with the straight-line Abel transform.

17. Key Words (Suggested by Author(s))	18. Distribution Statement
Occultation Profile inversion Radio physics	Unclassified – Unlimited

19. Security Classif. (of this report)	20. Security Classif. (of this page)	21. No. of Pages	22. Price*
Unclassified	Unclassified	31	$3.00

*For sale by the National Technical Information Service, Springfield, Virginia 22151

A COMPARISON OF TECHNIQUES FOR INVERSION OF RADIO-RAY PHASE DATA IN PRESENCE OF RAY BENDING

By H. Andrew Wallio and Mario D. Grossi*
Langley Research Center

SUMMARY

Derivations are presented of the straight-line Abel transform and the seismological Herglotz-Wiechert transform (which takes into account ray bending) that are used in the reconstruction of refractivity profiles from radio-wave phase data. Profile inversion utilizing these approaches, performed in computer-simulated experiments, are compared for cases of positive, zero, and negative ray bending. For thin atmospheres and ionospheres, such as the Martian atmosphere and ionosphere, radio-wave signals are shown to be inverted accurately with both methods. For dense media, such as the solar corona or the lower Venus atmosphere, the refractivities recovered by the seismological Herglotz-Wiechert transform provide a significant improvement compared with the straight-line Abel transform.

INTRODUCTION

Radio occultation measurements of planetary atmospheres and ionospheres have been an integral part of the standard scientific investigations performed with planetary space probes since the Mariner series of the mid-1960's. The Mariner IV spacecraft provided the first reliable measurements of the atmosphere and ionosphere of Mars by this technique in 1965. (See refs. 1 to 3.) Similarly, the Mariner V spacecraft provided refractivity profiles for Venus. (See refs. 4 to 6.)

One of the basic observables used in these experiments is the observed frequency of the radio signal received from the spacecraft. This frequency is compared with a fixed stable oscillator to derive an observed Doppler signal. By subtracting the amount of shift expected from the spacecraft-Earth link geometric changes from the observed Doppler signal, a "Doppler shift residual" is determined. For situations in which both link terminals are outside the medium being probed, the presence of a nonzero residual indicates a change of the emitted and/or received angle of the ray that propagates between

*Consulting Scientist, Raytheon Company, Sudbury, Mass.

the links and through the atmosphere of the planet being probed. The inversion problem is to obtain the atmospheric refractivity profile as a function of radial distance from the planetary center of mass from the observed Doppler shift and/or Doppler shift residuals. From the refractivity profile and certain assumptions about the constituents of the atmosphere and the planetary magnetic field, such atmospheric properties as the electron number density and its distributions, pressure, temperature, density, neutral number density, and their radial dependence can be deduced.

In the past, the inversion of the data has been performed with a variety of geometric optics techniques ranging from the closed-form Abel transform (based on the assumptions that the medium possesses spherical symmetry and based on the additional hypothesis, generally accepted by occultation experimenters, that there is straight-line ray travel (ref. 7)) to ray trace model-fitting approaches (based on iterative model update schemes (ref. 8)). For a planet with a thin atmosphere, such as Mars, all these methods are, in principle, adequate approximations to the ray-propagation theory. For dense media, like the atmospheres of Jupiter and Venus or the Sun corona where ray bending is large, closed-form inversion algorithms which utilize a straight-line ray approximation are inadequate. A suitable method to solve the problem in these cases is available from seismology and is based on the Herglotz-Wiechert approach for interpreting seismic data. (See refs. 9 and 10.)

In seismology, this bent-ray-path technique leads to the derivation of velocity-depth profiles and to the calculation of the position and the identification of geological features in the Earth's mantle. The observables are the travel times of seismic waves between stations located at known positions on the Earth's surface. Phinney and Anderson (ref. 11) have shown that this method is applicable to situations where the observables are the Doppler residuals of the radio occultation measurements. This method has been independently derived, programed, and applied to the Martian atmosphere (ref. 12) and this report is an extension of this earlier work to include denser atmospheres.

The purposes of this paper are to present the equations of the closed-form straight-line Abel transform and the Herglotz-Wiechert transform, and to compare the refractivities and minimum probing radius recovered by the two transforms for various cases of ray bending.

SYMBOLS

A	amplitude factor of electric field wave, $V\text{-}m^{-1}$
a,x,Z	limits of integration

c	speed of light, $km\text{-}sec^{-1}$
D	Doppler shift, sec^{-1}
D_{atm}	Doppler shift due to atmosphere, sec^{-1}
D_e	Doppler shift of unperturbed radio ray, sec^{-1}
$d\ell$	differential actual radio ray-path length, km
$d\ell'$	differential straight-line radio ray-path length, km
dr	differential of r, km
dS	differential of S, km
$d\theta$	differential of θ, deg
$\vec{E}$	electric field vector, $V\text{-}m^{-1}$
f	frequency of radio wave, sec^{-1}
G	phase factor of electric field wave
G_i	imaginary part of complex G
G_r	real part of complex G
$g(x), g'(x), \xi, \mu$	dummy functions used to illustrate Abel's integral equation
i	incidence angle, deg
K	propagation constant, km^{-1}
K_o	propagation constant in free space, km^{-1}
L	total path length, km
ℓ	actual radio ray-path length, km

ℓ'	straight-line radio ray-path length, km
N	refractivity, $10^6(n - 1)$
N_p	refractivity at minimum radial distance of radio ray
n	index of refraction
n_p	index of refraction at minimum radial distance of radio ray
p	impact parameter, km
r	radial distance from planetary center of mass, km
r_0	starting position of radio ray, km
r_p	radial distance of minimum point of radio ray, km
S	position of spacecraft on trajectory, km
$\dot{S}$	spacecraft velocity along trajectory projection, $km\text{-}sec^{-1}$
T,t,x	defined dummy variables
$T' = \frac{dT(\rho)}{d\rho}$	
α_e	geometric angle (see fig. 3), deg
β	variable between 0 and 1 used in Abel's integral equation
δ	deviation angle, deg
ϵ	inductive capacity, $N^{-1}(C\text{-}m^{-1})^2$
η	defined variable, km
η_0	starting value of η for a given ray, km
η_p	minimum value of η for a given ray, km

θ	unit of angular measure (see fig. 2), deg
λ	wavelength, km
ρ	perpendicular miss distance, km
ϕ	angular measure of phase cycles
ϕ_a	defined ray residual, cycles
ϕ_u	geometric phase term, cycles
ψ	radio-wave emission angle (see fig. 3), deg
ψ_e	unperturbed radio-ray emission angle (see fig. 3), deg

Subscripts:

0	starting position
L	last position of integration

ANALYSIS

Straight-Ray Abel Inversion Transform

The differential phase-path length is the difference between the straight-line geometrical distance between transmitter and receiver and the phase-path length for radio waves and is obtained from an integration in time of the Doppler residuals. The integration constant is zero when provisions are made for starting the integration from a position time where the probing link is completely external to the medium under investigation.

Figure 1 depicts the straight-ray Abel transform geometry. By assuming that the index of refraction is a spherically symmetric function,

$$\text{Differential phase-path length} = \int_{-\infty}^{\infty} d\ell' - \int_{-\infty}^{\infty} n(r)\, d\ell \tag{1}$$

By assuming that the radio-wave ray path is a straight line and sufficiently close to the geometric straight line that $d\ell \approx d\ell'$,

$$\text{Differential phase-path length} = \int_{-\infty}^{\infty} \left[1 - n(r)\right] d\ell' \tag{2}$$

The integral is a function of the distance of the ray from the center of the planet at the point of its closest approach.

Define

$$T(\rho) \equiv \int_{-\infty}^{+\infty} \left[1 - n(r)\right] d\ell' \tag{3}$$

Then, by changing the variable $d\ell'$ (see fig. 1),

$$T(\rho) = 2\int_{\rho}^{\infty} \frac{\left[1 - n(r)\right] r\, dr}{\sqrt{r^2 - \rho^2}} = -2\left(10^{-6}\right) \int_{\rho}^{\infty} \frac{N(r) r\, dr}{\sqrt{r^2 - \rho^2}} \tag{4}$$

In this equation the radicand in the denominator is nonnegative, because for every value of the miss-distance range ρ of the ray from the center of the planet, $r > \rho$.

Let $t \equiv \frac{1}{r^2}$ and $2r\, dr = -\frac{1}{t^2}\, dt$. Equation (4) becomes

$$T(\rho) = \int_{1/\rho^2}^{0} \frac{10^{-6} N\left(\frac{1}{\sqrt{t}}\right) dt}{t^2\sqrt{\frac{1}{t} - \rho^2}} = \int_{0}^{1/\rho^2} - \frac{10^{-6} N\left(\frac{1}{\sqrt{t}}\right) dt}{\rho t^{3/2}\sqrt{\frac{1}{\rho^2} - t}} \tag{5}$$

Let $x \equiv \frac{1}{\rho^2}$ and $\rho = \sqrt{\frac{1}{x}}$; then equation (5) becomes

$$\frac{1}{\sqrt{x}}\, T\left(\frac{1}{\sqrt{x}}\right) = \int_{0}^{x} - \frac{10^{-6} N\left(\frac{1}{\sqrt{t}}\right) dt}{t^{3/2}\sqrt{x - t}} \tag{6}$$

Applying Abel's integral equation in the form given in reference 13 as if

$$g(x) = \int_{a}^{x} \frac{\mu(\xi)\, d\xi}{(x - \xi)^{\beta}}$$

then

$$\mu(Z) = \frac{\sin \beta\pi}{\pi} \int_a^Z \frac{g'(x)\, dx}{(Z - x)^{1-\beta}}$$

(under the appropriate conditions as given in ref. 13) to equation (6) results in

$$\frac{N\left(\frac{1}{\sqrt{t}}\right)}{t^{3/2}} = -\frac{10^6}{\pi} \int_0^t \frac{\frac{d}{dx}\left[\frac{1}{\sqrt{x}}\, T\left(\frac{1}{\sqrt{x}}\right)\right]}{\sqrt{t - x}}\, dx \tag{7}$$

Let $t \equiv \frac{1}{r^2}$ and then equation (7) becomes

$$-r^3 N(r) = \frac{10^6}{\pi} \int_0^{1/r^2} \frac{\frac{d}{dx}\left[\frac{1}{\sqrt{x}}\, T\left(\frac{1}{\sqrt{x}}\right)\right]}{\sqrt{\frac{1}{r^2} - x}}\, dx \tag{8}$$

Now

$$\frac{d}{dx}\left[\frac{1}{\sqrt{x}}\, T\left(\frac{1}{\sqrt{x}}\right)\right] = -\frac{1}{2} \frac{T\left(\frac{1}{\sqrt{x}}\right)}{x^{3/2}} - \frac{1}{2} \frac{T'\left(\frac{1}{\sqrt{x}}\right)}{x^2} \tag{9}$$

so that equation (8) becomes

$$r^3 N(r) = \frac{10^6}{2\pi} \int_0^{1/r^2} \frac{\frac{T\left(\frac{1}{\sqrt{x}}\right)}{x^{3/2}} + \frac{T'\left(\frac{1}{\sqrt{x}}\right)}{x^2}}{\sqrt{\frac{1}{r^2} - x}}\, dx \tag{10}$$

where $T' = \frac{dT(\rho)}{d\rho}$. Let $x = \frac{1}{\rho^2}$ and $2\rho\, d\rho = -\frac{1}{x^2}\, dx$; then equation (10) becomes

$$r^3 N(r) = -\frac{10^6}{2\pi} \int_\infty^r \frac{\left[\frac{T(\rho)}{\rho} + T'(\rho)\right] 2\rho\, d\rho}{\sqrt{\frac{1}{r^2} - \frac{1}{\rho^2}}} \tag{11}$$

or rewritten

$$N(r) = \frac{10^6}{\pi r^2} \int_r^\infty \frac{\rho T(\rho) + \rho^2 T'(\rho)}{\sqrt{\rho^2 - r^2}} \, d\rho \tag{12}$$

and

$$n(r) = 1 + \frac{1}{\pi r^2} \int_r^\infty \frac{\rho T(\rho) + \rho^2 T'(\rho)}{\sqrt{\rho^2 - r^2}} \, d\rho \tag{13}$$

Because of the change in the limits of integration, the radicand in the denominator is nonnegative. In fact, for every radial height r, $N(r)$ and $n(r)$ are obtained from columnar measurements made at miss distances ρ always larger than r.

Thus, under certain restrictive assumptions, the index of refraction of the medium being probed is shown to be a function of the differential phase-path length and its derivative which are known observables.

Herglotz-Wiechert or Seismic Inversion Transform

In seismology, the observable is the central angle θ subtended by seismic wave rays in the Earth. (See fig. 2.) The analytical steps are arranged in such a way that the velocity-depth profiles are obtained by operations on θ.

In radio occultation measurements, the observables are the Doppler shift residuals so that the theory used in seismology must be modified so that the refractivity or index-of-refraction profiles are obtained by operations on the Doppler shift residuals. The important aspect of the Herglotz-Wiechert approach is that the straight-line ray approximation is not required.

The geometry of the occultation is shown in figure 2. The index of refraction n is assumed to be a radially dependent function, and from Fermat's principle, the first variation of the phase-path length should be zero,

$$\delta \int n \, d\ell = 0 \tag{14}$$

where $d\ell^2 = dr^2 + r^2 \, d\theta^2$. The Euler-Lagrange equation which yields a minimum for equation (14) is

$$\frac{nr^2 \frac{d\theta}{dr}}{\left[1 + r^2 \left(\frac{d\theta}{dr}\right)^2\right]^{1/2}} = \text{Constant} \tag{15}$$

and from the boundary conditions at the minimum radius, Snell's law in spherical geometry is determined, that is,

$$p = nr \sin i = n_p r_p \equiv \text{Impact parameter} \tag{16}$$

The impact parameter is a constant for a given ray.

Define the variable η as

$$\eta = nr = \frac{p}{\sin i} \tag{17}$$

From the definition of the path length

$$L = \int d\ell = \int \left[1 + r^2 \left(\frac{d\theta}{dr}\right)^2\right]^{1/2} dr \tag{18}$$

and the application of equations (15) to (17), the integral function for the path length is found to be

$$L = 2 \int_{r_p}^{r} nr\left(\eta^2 - p^2\right)^{-1/2} dr \tag{19}$$

The phase (angular measure) along the ray path is

$$\phi = \frac{f}{c} \int n \, d\ell \tag{20}$$

and by using equations (17) and (19),

$$\phi(p) = 2\frac{f}{c} \int_{r_p}^{r_0} \frac{\eta^2}{r}\left(\eta^2 - p^2\right)^{-1/2} dr \tag{21}$$

By applying the operator L to equation (21) where

$$L(f) = \int_{\eta_1}^{\eta_0} fp\left(p^2 - \eta_1{}^2\right)^{-1/2} dp \tag{22}$$

and where $\eta_0 \geqq \eta_1 \geqq \eta_p$ by integrating over p, by interchanging the order of integration, by integrating by parts repeatedly, and by performing a final integration over the appropriate regions, the phase function (eq. (21)) can be shown to be inverted (see appendix) to

$$r_p = r_0 \exp\left\{-\frac{c}{\pi f}\int_{\eta_0}^{\eta} \cosh^{-1}\left[\frac{p}{p(\eta)}\right]\frac{1}{p}\frac{d\phi}{dp}\,dp\right\} \tag{23}$$

Thus, the refractivity is found as

$$N_p = 10^6\left(\frac{p(\eta)}{r_0 \exp\left\{-\frac{c}{\pi f}\int_{\eta_0}^{\eta} \cosh^{-1}\left[\frac{p}{p(\eta)}\right]\frac{1}{p}\frac{d\phi}{dp}\,dp\right\}} - 1\right) \tag{24}$$

By following Phinney and Anderson (ref. 11), if a ray residual ϕ_a is defined as

$$\phi_a = \phi - \phi_u \tag{25}$$

where ϕ_u is a geometric term, then

$$N_p = 10^6\left(\exp\left\{\frac{c}{\pi f}\int_{x_0}^{x_L} \cosh^{-1}\left[\frac{p(x)}{p(x_L)}\right]\frac{1}{p(x)}\frac{d\phi_a}{dx}\,dx\right\} - 1\right) \tag{26}$$

where x is a dummy variable such as time to occultation or satellite position.

Thus, if the impact parameter p (eq. (16)) can be determined, the minimum probing radius and the refractivity at that radius are determined for each radio-wave ray as a function of the known differential phase path by equations (23) and (26), respectively.

Determination of Impact Parameter

In order to evaluate the impact parameter, a ray-optical treatment is considered from an Earth-centered coordinate system. The spacecraft is thought of as sampling phase along an arc through a family of constant phase surfaces and the radio waves are emitted orthogonally to these surfaces.

Then the equation for the directional derivative (ref. 14) is

$$\frac{d\vec{r}}{dS} \cdot \nabla\phi = \frac{d\phi}{dS} \tag{27}$$

where $d\vec{r}$ is the tangent line to the projection of the spacecraft trajectory in the plane of the spacecraft, planet, and Earth at any point S along the trajectory, $d\vec{r}/dS$ is a unit vector, and $\nabla\phi$ is the direction of propagation.

Therefore, the angle between the radio ray and trajectory becomes (see fig. 3)

$$\cos \psi = \frac{d\phi}{dS} \left|\nabla\phi\right|^{-1} \tag{28}$$

In order to evaluate the radio-ray emission angle ψ from the directional derivative, the gradient of the phase $\nabla\phi$ or the eiconal equation must be determined. To determine this equation, assume a nonconducting isotropic medium where the inductive capacity ϵ is a function of position. Then the wave equation for the electric field vector becomes

$$\nabla^2\vec{E} + K^2\vec{E} = -\nabla\left(\vec{E} \cdot \frac{\nabla\epsilon}{\epsilon}\right) = \nabla^2\vec{E} + K_o{}^2 n^2 \vec{E} \tag{29}$$

where $K_o = f/c$ is the propagation constant measured in cycles. If it is assumed that the spatial change of ϵ is small compared with a wavelength

$$\left|\frac{\nabla\epsilon}{\epsilon}\right| << \frac{1}{\lambda} \tag{30}$$

then the wave equation reduces to its homogeneous form

$$\nabla^2\vec{E} + K_o{}^2 n^2 \vec{E} = 0 \tag{31}$$

Assume that the form of the solution is

$$E = Ae^{-iK_oG} \tag{32}$$

where $G = G_r + iG_i$ so that surfaces of G_r = Constant are surfaces of constant phase and surfaces of G_i = Constant, are surfaces of constant amplitude. Substitution of equation (32) into equation (31) yields

$$\nabla^2 A + K_o{}^2 A\left[n^2 - (\nabla G)^2\right] - iK_o\left[A\nabla^2 G + 2\left(\vec{\nabla}A\right) \cdot \left(\vec{\nabla}G\right)\right] = 0 \tag{33}$$

If K_o is large in the sense that

$$\nabla^2 A << K_o{}^2 \tag{34}$$

and

$$A\nabla^2 G + 2\left(\vec{\nabla}A\right) \cdot \left(\vec{\nabla}G\right) << K_o \tag{35}$$

(therefore regions of diffraction, focal points, caustics, and sources are excluded), then

$$(\nabla G)^2 = n^2 \tag{36}$$

Now $K_o G = \phi + ft$ for a real η so that

$$(\nabla \phi)^2 = \left(\frac{f}{c} n\right)^2 \tag{37}$$

which is the eiconal equation.

Since n is a function of position if the spacecraft shown in figure 3 is inside the planetary atmosphere, the profile of the atmosphere must be known before equation (37) can be solved for $|\nabla \phi|$.

If, however, the spacecraft is above the atmosphere, then n becomes unity and equation (37) becomes

$$(\nabla \phi)^2 = \left(\frac{f}{c}\right)^2 \tag{38}$$

Substituting equation (38) into equation (37) yields

$$\cos \psi = \frac{c}{f} \frac{d\phi}{dS} \tag{39}$$

By letting time be the independent variable and D signify an instantaneous Doppler shift,

$$\frac{d\phi}{dS} = \frac{1}{\dot{S}} \frac{d\phi}{dt} = \frac{D}{\dot{S}} \tag{40}$$

Then D can be thought of as being composed of two parts

$$D = D_e + D_{atm} \tag{41}$$

where D_e is the expected geometric Doppler shift from the predicted trajectory and D_{atm} is the residual normally attributed to the atmosphere. Therefore,

$$\cos \psi = \frac{c}{f\dot{S}} \left(D_e + D_{atm}\right) \tag{42}$$

If there is no atmosphere

$$\cos \psi_e = \frac{c}{f\dot{S}} D_e \tag{43}$$

where ψ_e is the angle between the trajectory tangent and the unperturbed ray or straight-line distance between the spacecraft and Earth.

Algebraic manipulation of equations (42) and (43) yields the deviation angle δ (fig. 3)

$$\delta = \psi - \psi_e = 2 \tan^{-1}\left\{\frac{\left[D_s^2 - (D_e + D_{atm})^2\right]^{1/2} - (D_s^2 - D_e^2)^{1/2}}{D_{atm} + 2D_e}\right\} \tag{44}$$

or

$$\delta = 2 \tan^{-1}\left[\frac{(D_s^2 - D^2)^{1/2} - (D_s^2 - D_e^2)^{1/2}}{D + D_e}\right] \tag{45}$$

where

D observed Doppler shift

D_{atm} Doppler residual due to atmosphere

D_e Doppler shift of unperturbed ray

$D_s = \frac{f}{c}\dot{S}$

Thus, the impact parameter for a ray is

$$p = r_s \sin(\alpha_e - \delta) \tag{46}$$

where

r_s distance of spacecraft from planet center of mass

α_e a known geometric angle (fig. 3)

Implied in equation (46) is the dependency of each ray impact parameter on either of the related variables of spacecraft position or time.

RESULTS AND DISCUSSION

A comparison is made of the recovered refractivity profiles obtained by using the straight-line Abel and Herglotz-Wiechert transforms. Three types of atmospheres have been used to compare the two forms of transforms: Venus (where the radio rays are bent positively inward by the neutral atmosphere); Mars (where ray bending is negligible); and the solar corona (where the rays are bent negatively outward by the electron plasma).

For this study it was assumed that the Earth-planet distance was sufficiently large to insure that the radio rays emerging from the atmosphere can be considered parallel. Therefore, all the observable atmospheric frequency shifts can be considered to arise from effects that have occurred between the spacecraft and an imaginary reference plane located between the Earth and the planet and beyond the sensible atmosphere. The phase data for the three models were generated, for a frequency of 2000 MHz, by a ray-tracing program; this program was a modified version of a program reported in reference 15.

The assumed Venus atmospheric model has a relatively small ionosphere component compared with the neutral layer. For this model, ray bending in the lower atmosphere is significant and the differences in the recovered parameters between the straight-line Abel and the seismic Herglotz-Wiechert approach are clearly noticeable. The recovered refractivity from the straight-line Abel (Abel), the seismic Herglotz-Wiechert (Seismic), and the model refractivity (Model) against the appropriate planetocentric radial position from Venus are plotted in figure 4 for the measured phase function.

In table I is a listing of the differences in the recovered refractivity and minimum probing radii of the two transform methods from the respective actual refractivity and minimum probing radius. From table I and figure 4, it can be seen that as the radio rays probe lower into the atmosphere and ray bending increases, the divergence of the recovered values increases, the seismic Herglotz-Wiechert method giving consistently better recovered values.

The Martian atmosphere model is similar to the one developed from the Mariner IV results. For this example, ray bending is small and the straight-line Abel transform has been shown in the past to be a fully adequate approximation. The recovered refractivity from the straight-line Abel transform (Abel), the seismic Herglotz-Wiechert transform (Seismic), and the model refractivity (Model) against geocentric radius of Mars are plotted in figure 5 for the measured phase function.

Table II is a listing of the differences in recovered refractivity and minimum probing radius of the two transform methods from the respective actual refractivity and minimum probing radius for Mars. From figure 5 or table II, it can be seen that the errors in the recovered refractivity of the two transforms are about the same. Also, the

minimum probing radius found by each transform is very close to the actual minimum probing radius because of the small amount of ray bending.

A Baumbach electron density model was used for the solar corona. For this case ray bending is again very large and the deviations between the classical straight-line Abel transform and the seismic Herglotz-Wiechert transform are clearly noticeable. The recovered refractivity from the straight-line Abel (Abel), the seismic Herglotz-Wiechert (Seismic), and the solar model refractivity (Model) against their respective heliocentric radial position are plotted in figure 6.

Table III is a listing of the differences in recovered refractivity and minimum probing radius of the two transform methods from the respective actual refractivity and minimum probing radius for the sun. From figure 6 or table III, it can be seen that the divergence of the recovered refractivities and minimum probing radii compared with the actual model values increases as the ray bending increases, the seismic Herglotz-Wiechert transform yielding the parameter values closest to the model values.

CONCLUDING REMARKS

The work reported herein has shown that profile inversion of phase data collected from strongly bent radio rays requires the use of techniques like the seismological Herglotz-Wiechert transform which do not rely on the validity of the straight-line approximation.

For highly refractive media like the solar corona or the lower Venus atmosphere, the recovered refractivities by the Herglotz-Wiechert transform provide significant improvement compared with the straight-line Abel transform (a reduction of refractivity error at the lowest probed altitude from over 60 percent to less than 20 percent for the solar corona and a reduction of error from 150 percent to 3 percent for the Venus lower atmosphere).

Langley Research Center,
National Aeronautics and Space Administration,
Hampton, Va., October 20, 1972.

APPENDIX

TRANSFORMATION OF PHASE EQUATION TO EQUATION FOR MINIMUM PROBING RADIUS

This appendix gives an outline of the mathematical steps used to transform the phase function (eq. (21)) to the equation for the value of the refractivity at the minimum point of the probing ray.

If the phase function (from eq. (21))

$$\phi(p) = 2\,\frac{f}{c}\int_p^{\eta_0} \frac{\eta^2}{r}\left(\eta^2 - p^2\right)^{-1/2}\frac{dr}{d\eta}\,d\eta \tag{A1}$$

is given, let r_1 be such that $r_0 \geqq r_1 \geqq R$, then $\eta_0 \geqq \eta_1 \geqq \eta_R$. Apply the kernel $p\left(p^2 - \eta_1{}^2\right)^{-1/2}$ to equation (A1) and integrate over p from η_1 to η_0 to yield

$$\int_{\eta_1}^{\eta_0} \frac{p\phi}{\sqrt{p^2 - \eta_1{}^2}}\,dp = 2\,\frac{f}{c}\int_{\eta_1}^{\eta_0} dp\left\{\int_p^{\eta_0} \frac{p\eta^2}{r}\left[\left(\eta^2 - p^2\right)\left(p^2 - \eta_1{}^2\right)\right]^{-1/2}\frac{dr}{d\eta}\,d\eta\right\} \tag{A2}$$

Interchanging the order of integration results in

$$\int_{\eta_1}^{\eta_0} \frac{p\phi\,dp}{\sqrt{p^2 - \eta_1{}^2}} = \frac{f}{c}\int_{\eta_1}^{\eta_0} \frac{\eta^2}{r}\frac{dr}{d\eta}\,d\eta\left[\int_{\eta_1}^{\eta_0} \frac{2p\,dp}{\sqrt{\left(p^2 - \eta_1{}^2\right)\left(\eta^2 - p^2\right)}}\right]$$

$$= \frac{f}{c}\int_{\eta_1}^{\eta_0} \pi\eta^2\,\frac{d\log_e r}{d\eta}\,d\eta \tag{A3}$$

which reduces to

$$\frac{\log_e r}{d\eta} = \frac{c}{\eta^2 \pi f}\,\frac{d}{d\eta}\left(\int_{\eta_1}^{\eta_0} \frac{p\phi\,dp}{\sqrt{p^2 - \eta_1{}^2}}\right) \tag{A4}$$

Let $\eta \rightarrow \mu$ and integrate both sides of equation (A4) over μ from η_0 to η to yield

$$\log_e\left[\frac{r(\eta)}{r_0}\right] = \frac{c}{\pi f}\int_{\eta_0}^{\eta} \frac{\frac{d}{d\mu}\left(\int_{\eta_1}^{\eta_0} \frac{p\phi\, dp}{\sqrt{p^2 - \eta_1^2}}\right)}{\mu^2}\, d\mu \tag{A5}$$

Let $\eta_1 \equiv \mu$ and then integrate equation (A5) by parts to yield

$$\log_e\left[\frac{r(\eta)}{r_0}\right] = \frac{c}{\pi f}\left(\frac{1}{\eta^2}\int_{\eta}^{\eta_0} \frac{p\phi\, dp}{\sqrt{p^2 - \eta^2}} - 2\int_{\eta}^{\eta_0} \frac{d\mu}{\mu^3}\int_{\mu}^{\eta_0} \frac{p\phi\, dp}{\sqrt{p^2 - \mu^2}}\right) \tag{A6}$$

Interchanging the order of integration and integrating with respect to μ result in

$$\log_e\left[\frac{r(\eta)}{r_0}\right] = \frac{c}{\pi f}\left[\frac{1}{\eta^2}\int_{\eta}^{\eta_0} \frac{p\phi\, dp}{\sqrt{p^2 - \eta^2}} - 2\int_{\eta}^{\eta_0} \phi p\, dp\left(-\frac{\sqrt{p^2 - \mu^2}}{2p^2\mu^2} - \frac{1}{2p^3}\cosh^{-1}\frac{p}{\mu}\right)\Bigg|_{\eta}^{p}\right] \tag{A7}$$

which reduces to

$$\log_e\left[\frac{r(\eta)}{r_0}\right] = \frac{c}{\pi f}\left\{\int_{\eta}^{\eta_0}\left[\frac{\phi p}{\eta^2\sqrt{p^2 - \eta^2}} - \frac{\phi\sqrt{p^2 - \eta^2}}{\eta^2 p} - \frac{\phi}{p^2}\cosh^{-1}\left(\frac{p}{\eta}\right)\right] dp\right\} \tag{A8}$$

The second term on the right-hand side of equation (A8) becomes, after integrating by parts,

$$-\frac{1}{\eta^2}\int_{\eta}^{\eta_0} \frac{\phi}{p}\sqrt{p^2 - \eta^2}\, dp = -\int_{\eta}^{\eta_0} \frac{\phi p}{\eta^2\sqrt{p^2 - \eta^2}}\, dp - \int_{\eta}^{\eta_0} \frac{1}{\eta}\cos^{-1}\left(\frac{\eta}{p}\right)\frac{d\phi}{dp}\, dp \tag{A9}$$

The third term on the right-hand side of equation (A8) becomes, after integrating by parts,

$$-\int_{\eta}^{\eta_0} \frac{\phi}{p^2}\cosh^{-1}\left(\frac{p}{\eta}\right) dp = -\left[\int_{\eta}^{\eta_0} \frac{1}{p}\frac{d\phi}{dp}\cosh^{-1}\left(\frac{p}{\eta}\right) dp - \int_{\eta}^{\eta_0} \frac{1}{\eta}\cos^{-1}\left(\frac{\eta}{p}\right)\frac{d\phi}{dp}\, dp\right] \tag{A10}$$

Combining equations (A10) and (A9) in equation (A8) yields

$$\log_e\left[\frac{r(\eta)}{r_0}\right] = \frac{c}{\pi f}\left(\int_{\eta}^{\eta_0}\left\{\frac{\phi p}{\eta^2\sqrt{p^2 - \eta^2}} - \frac{\phi p}{\eta^2\sqrt{p^2 - \eta^2}} - \frac{1}{\eta}\cos^{-1}\left(\frac{\eta}{p}\right)\frac{d\phi}{dp}\right.\right.$$

$$\left.\left. - \left[\frac{1}{p}\frac{d\phi}{dp}\cosh^{-1}\left(\frac{p}{\eta}\right) - \frac{1}{\eta}\cos^{-1}\left(\frac{\eta}{p}\right)\frac{d\phi}{dp}\right]\right\} dp\right) \tag{A11}$$

Equation (A11) reduces to

$$r(\eta) = r_0 \exp\left[\frac{c}{\pi f}\int_{\eta_0}^{\eta}\cosh^{-1}\left(\frac{p}{\eta}\right)\frac{1}{p}\frac{d\phi}{dp}\,dp\right] \tag{A12}$$

and since $r(\eta) \leqq r_0$, the negative value of double-valued $\cosh^{-1}\left(\frac{p}{\eta}\right)$ must be taken.

At the "turning point" in the atmosphere (where $\sin i = 1$)

$$\eta_p = p = r_0 \sin i_0 = n_p r_p \tag{A13}$$

Therefore, transforming equation (A12) to a dummy variable dependence and using equation (A13)

$$r_p = r_0 \exp\left\{-\frac{c}{\pi f}\int_{x_0}^{x_L}\cosh^{-1}\left[\frac{p(x)}{p(x_L)}\right]\frac{1}{p(x)}\frac{d\phi}{dx}\,dx\right\} \tag{A14}$$

Using equation (A13) again yields

$$n_p = \sin i_0\left(\exp\left\{\frac{c}{\pi f}\int_{x_0}^{x_L}\cosh^{-1}\left[\frac{p(x)}{p(x_L)}\right]\frac{1}{p(x)}\frac{d\phi}{dx}\,dx\right\}\right) \tag{A15}$$

Now $\phi \equiv \phi_a + \phi_\mu$ so that if there is no atmosphere, $\phi = \phi_\mu$ and equation (A15) becomes

$$1 = \sin i_0\left(\exp\left\{\frac{c}{\pi f}\int_{x_0}^{x_L}\cosh^{-1}\left[\frac{p(x)}{p(x_L)}\right]\frac{1}{p(x)}\frac{d\phi_\mu}{dx}\,dx\right\}\right) \tag{A16}$$

and therefore

$$N_p = 10^6\left(\exp\left\{\frac{c}{\pi f}\int_{x_0}^{x_L}\cosh^{-1}\left[\frac{p(x)}{p(x_L)}\right]\frac{1}{p(x)}\frac{d\phi_a}{dx}\,dx\right\} - 1\right) \tag{A17}$$

which is equation (26).

REFERENCES

1. Kliore, Arvydas; Cain, Dan L.; Levy, Gerald S.; Eshleman, Von R.; Fjeldbo, Gunnar; and Drake, Frank D.: Occultation Experiment: Results of the First Direct Measurements of Mars's Atmosphere and Ionosphere. Science, vol. 149, no. 3689, Sept. 1965, pp. 1243-1248.

2. Fjeldbo, Gunnar; Fjeldbo, Wencke C.; and Eshleman, Von R.: Models for the Atmosphere of Mars Based on Mariner 4 Occultation Experiment. J. Geophys. Res., vol. 71, no. 9, May 1966, pp. 2307-2316.

3. Fjeldbo, Gunnar; and Eshleman, Von R.: The Atmosphere of Mars Analyzed by Integral Inversion of the Mariner IV Occultation Data. Planet. Space Sci., vol. 16, no. 8, Aug. 1968, pp. 1035-1059.

4. Kliore, Arvydas; Levy, Gerald S.; Cain, Dan L.; Fjeldbo, Gunnar; and Rasool, S. I.: Atmosphere and Ionosphere of Venus From the Mariner V S-Band Radio Occultation Measurement. Science, vol. 158, no. 3809, Dec. 1967, pp. 1683-1688.

5. Mariner Stanford Group: Venus: Ionosphere and Atmosphere as Measured by Dual-Frequency Radio Occultation of Mariner V. Science, vol. 158, no. 3809, Dec. 1967, pp. 1678-1683.

6. Fjeldbo, G.; and Eshleman, V. R.: Atmosphere of Venus as Studied With the Mariner 5 Dual Radio-Frequency Occultation Experiment. Radio Science, vol. 4, no. 10, Oct. 1969, pp. 879-897.

7. Harrington, J. V.; Grossi, M. D.; Goff, R. W.; and Langworthy, B. M.: Radio Occultation Measurements of Planetary Atmospheres and Ionospheres From an Orbiting Pair. AIAA Paper No. 69-53, Jan. 1969.

8. Kliore, Arvydas; Cain, Dan L.; Levy, Gerald S.; Fjeldbo, Gunnar; and Rasool, S. I.: Structure of the Atmosphere of Venus Derived From Mariner V S-Band Measurements. Space Research IX, K. S. W. Champion, P. A. Smith, and R. L. Rose-Smith, eds., North-Holland Pub. Co., 1969, pp. 712-729.

9. Herglotz, G.: Propagation of Earthquake Shocks Within the Earth. Phys. Zeitschr., vol. 8, Mar. 1, 1907, pp. 145-147.

10. Wiechert, E.; and Geiger, L.: Paths of Seismic Waves. Phys. Zeitschr., vol. 11, Apr. 1, 1910, pp. 294-311.

11. Phinney, R. A.; and Anderson, D. L.: On the Radio Occultation Method for Studying Planetary Atmospheres. J. Geophys. Res., vol. 73, no. 5, Mar. 1, 1968, pp. 1819-1827.

12. Wallio, H. A.; and Grossi, M. D.: Profile Inversion in Presence of Ray Bending. Proceedings of Workshop on Mathematics of Profile Inversion, L. Colin, ed., NASA TM X-62150, 1972.

13. Bôcher, Maxime: An Introduction to the Study of Integral Equations. Hafner Pub. Co., 1913.

14. Hildebrand, Francis B.: Advanced Calculus for Applications. Prentice-Hall, Inc., 1962.

15. Anon.: Electromagnetic Probing of the Mars and Venus Atmospheres and Ionospheres From an Orbiting Pair. Vol. I. R69-4373-1(Contract NASW-1772), Raytheon Co., Sept. 19, 1969. (Available as NASA CR-106809.)

16. Anon.: Electromagnetic Probing of the Mars and Venus Atmospheres and Ionospheres From an Orbiting Pair. Vol. II. R69-4373-2 (Contract NASW-1772), Raytheon Co., Dec. 19, 1969. (Available as NASA CR-106808.)

TABLE I.- ORIGINAL AND RECONSTRUCTED MODEL FOR ATMOSPHERE AND IONOSPHERE OF VENUS

[Reconstructed by Abel transform and Herglotz-Wiechert transform]

		ABEL			HERGLOTZ-WIECHERT		
PLANETOCENTRIC RADIUS (km)	MODEL REFRACTIVITY (N Units)	REFRACTIVITY CALCULATED (N Units)	REFRACTIVITY DIFFERENCE (N Units)	MINIMUM RADIUS DIFFERENCE (km)	REFRACTIVITY CALCULATED (N Units)	REFRACTIVITY DIFFERENCE (N Units)	MINIMUM RADIUS DIFFERENCE (km)
6.094602E+03	1.558703E+03	3.900569E+03	2.341861E+03	8.401381E+01	1.607844E+03	4.913613E+01	-3.078891E-01
6.101996E+03	1.000250E+03	2.007955E+03	1.007706E+03	4.907713E+01	9.952482E+02	-5.001364E+00	2.013005E-02
6.108411E+03	6.043893E+02	1.138644E+03	5.342542E+02	3.364625E+01	6.142947E+02	9.905422E+00	-8.173213E-02
6.114108E+03	3.184412E+02	4.975987E+02	1.791576E+02	1.813688E+01	3.249528E+02	6.511665E+00	-4.793382E-02
6.119143E+03	1.585259E+02	2.060523E+02	4.752636E+01	9.135010E+00	1.614589E+02	2.932977E+00	-3.633740E-02
6.123667E+03	7.488796E+01	8.347060E+01	8.582646E+00	4.379980E+00	7.537021E+01	4.822546E-01	-1.629867E-02
6.127921E+03	3.343338E+01	3.346262E+01	9.242554E-03	1.996860E+00	3.272604E+01	-7.273396E-01	-1.276945E-02
6.132049E+03	1.394535E+01	1.311992E+01	-8.254293E-01	8.441800E-01	1.249991E+01	-1.445438E+00	-3.201034E-03
6.136109E+03	5.392480E+00	5.229405E+00	-1.630753E-01	3.056600E-01	3.357684E+00	-2.034796E+00	-1.241998E-03
6.140141E+03	0.	1.624730E-02	1.624730E-02	9.000002E-05	-1.476682E-01	-1.476682E-01	5.809902E-05
6.144147E+03	0.	-1.296716E-02	-1.296716E-02	3.400000E-04	-1.466982E-01	-1.466982E-01	-3.292927E-05
6.148154E+03	0.	3.898800E-03	3.898800E-03	2.500000E-04	-1.465804E-01	-1.465804E-01	5.555671E-05
6.152161E+03	0.	-3.600030E-03	-3.600030E-03	5.000000E-04	-1.460501E-01	-1.460501E-01	3.003338E-05
6.156168E+03	0.	5.844104E-03	5.844104E-03	4.200000E-04	-1.468374E-01	-1.468374E-01	6.687653E-05
6.160174E+03	0.	-6.744457E-03	-6.744457E-03	8.500000E-04	-1.463040E-01	-1.463040E-01	9.393305E-05
6.164181E+03	0.	1.545986E-02	1.545986E-02	7.600000E-04	-1.490878E-01	-1.490878E-01	1.160978E-04
6.168187E+03	0.	-5.867549E-02	-5.967549E-02	1.870000E-03	-1.513026E-01	-1.513026E-01	1.966636E-04
6.172194E+03	-1.478406E-01	-1.483956E-01	-5.549336E-04	2.160000E-03	-1.742662E-01	-2.642558E-02	8.803629E-05
6.176201E+03	-1.643749E-01	-1.738990E-01	-5.149930E-03	1.170000E-03	-2.059671E-01	-3.721811E-02	3.224952E-05
6.180208E+03	-1.846543E-01	-1.868845E-01	-2.229658E-03	2.600000E-04	-2.295207E-01	-4.486588E-02	7.609051E-05
6.184215E+03	-1.952000E-01	-1.952349E-01	-3.495948E-05	5.230000E-04	-2.457158E-01	-5.051584E-02	7.750926E-05
6.188221E+03	-2.008660E-01	-2.041446E-01	-3.548593E-03	-1.130000E-03	-2.542565E-01	-5.366048E-02	3.882754E-05
6.192228E+03	-2.014268E-01	-2.024269E-01	-1.000140E-03	-1.580000E-03	-2.554193E-01	-5.399251E-02	7.179682E-05
6.196235E+03	-1.994673E-01	-1.973641E-01	1.103177E-03	-1.880000E-03	-2.514100E-01	-5.294270E-02	7.096305E-05
6.200241E+03	-1.925442E-01	-1.911801E-01	1.364133E-03	-2.040000E-03	-2.429679E-01	-5.042370E-02	3.308212E-05
6.204248E+03	-1.844436E-01	-1.838575E-01	5.461707E-04	-2.110000E-03	-2.306203E-01	-4.617665E-02	6.269460E-05
6.208255E+03	-1.748592E-01	-1.745877E-01	2.715273E-04	-2.080000E-03	-2.164542E-01	-4.159491E-02	6.472380E-05
6.212261E+03	-1.643705E-01	-1.628910E-01	1.479463E-03	-2.000000E-03	-2.009933E-01	-3.662285E-02	5.586122E-05
6.216268E+03	-1.534401E-01	-1.516090E-01	1.831049E-03	-1.880000E-03	-1.847582E-01	-3.131812E-02	5.452186E-05
6.220274E+03	-1.424236E-01	-1.420076E-01	4.160424E-04	-1.750000E-03	-1.684009E-01	-2.597721E-02	5.402154E-05
6.224281E+03	-1.315638E-01	-1.290483E-01	2.535506E-03	-1.590000E-03	-1.522638E-01	-2.067996E-02	5.399485E-05
6.228287E+03	-1.211063E-01	-1.195762E-01	1.530113E-03	-1.430000E-03	-1.367364E-01	-1.563012E-02	4.668889E-05
6.232294E+03	-1.111158E-01	-1.109581E-01	1.576335E-04	-1.280000E-03	-1.218493E-01	-1.073352E-02	3.912699E-05
6.236301E+03	-1.016894E-01	-1.011017E-01	5.877328E-04	-1.130000E-03	-1.077207E-01	-6.031264E-03	3.472780E-05
6.240307E+03	-9.286833E-02	-9.221419E-02	6.541469E-04	-9.700000E-04	-9.442856E-02	-1.560231E-03	9.009615E-06
6.244314E+03	-8.466746E-02	-8.433053E-02	3.369295E-04	-8.400000E-04	-8.186492E-02	2.802537E-03	8.372474E-06
6.248320E+03	-7.708274E-02	-7.326189E-02	-1.179148E-03	-7.200000E-04	-7.015859E-02	6.924147E-03	3.949361E-06
6.252327E+03	-7.009712E-02	-7.268697E-02	-2.589853E-03	-6.100000E-04	-5.917345E-02	1.092366E-02	-3.104680E-06
6.256333E+03	-6.368480E-02	-7.360722E-02	-6.922419E-03	-5.200000E-04	-4.841868E-02	1.526612E-02	-1.784394E-05
6.260340E+03	-5.781464E-02	-5.171525E-02	6.099385E-03	-4.430000E-04	-3.816398E-02	1.965066E-02	8.909538E-05
6.264347E+03	-5.245256E-02	-5.166167E-02	7.908823E-04	-3.400000E-04	-3.094580E-02	2.150676E-02	4.033188E-05
6.268353E+03	-4.756734E-02	-4.731094E-02	-2.475047E-04	-2.800000E-04	-2.353161E-02	2.403173E-02	6.245292E-05
6.272360E+03	-4.311171E-02	-4.428998E-02	-1.178273E-03	-2.100000E-04	-1.698147E-02	2.613024E-02	4.517977E-05
6.276367E+03	-3.906325E-02	-4.426401E-02	-5.200770E-03	-1.400000E-04	-1.059254E-02	2.847071E-02	6.644014E-05
6.280373E+03	0.	5.158079E-04	5.158079E-04	0.	-6.502397E-03	-6.502397E-03	4.059557E-05
6.284380E+03	0.	5.867231E-04	5.867231E-04	0.	-6.330332E-03	-6.330332E-03	4.025092E-05
6.288387E+03	0.	6.956671E-04	6.956671E-04	0.	-6.056389E-03	-6.056389E-03	3.824843E-05
6.292393E+03	0.	9.114577E-04	9.114577E-04	0.	-5.566918E-03	-5.566918E-03	3.485451E-05
6.296400E+03	0.	2.276148E-03	2.276148E-03	0.	-3.966811E-03	-3.966811E-03	2.451360E-05
6.300000E+03	0.	0.	0.	1.100000E-03	-0.	0.	1.000000E-04

TABLE II.- ORIGINAL AND RECONSTRUCTED MODEL FOR ATMOSPHERE AND IONOSPHERE OF MARS

[Reconstructed by Abel transform and Herglotz-Wiechert transform]

		ABEL			HERGLOTZ-WIECHERT		
PLANETOCENTRIC RADIUS (km)	MODEL REFRACTIVITY (N Units)	REFRACTIVITY CALCULATED (N Units)	REFRACTIVITY DIFFERENCE (N Units)	MINIMUM RADIUS DIFFERENCE (km)	REFRACTIVITY CALCULATED (N Units)	REFRACTIVITY DIFFERENCE (N Units)	MINIMUM RADIUS DIFFERENCE (km)
3.385898E+03	2.691001E+00	2.534333E+00	-1.566678E-01	9.452920E-02	2.763462E+00	7.246107E-02	-1.365307E-04
3.390811E+03	1.296938E+00	1.112744E+00	-1.841937E-01	5.666340E-02	1.504153E+00	2.072156E-01	-5.960265E-04
3.395720E+03	7.342651E-01	7.000476E-01	-3.421752E-02	2.267790E-02	7.541950E-01	1.992988E-02	4.000985E-05
3.400629E+03	4.823507E-01	4.507898E-01	-3.156054E-02	1.728530E-02	5.022356E-01	1.988509E-02	4.053678E-05
3.405537E+03	2.818809E-01	2.533988E-01	-2.846213E-02	1.247690E-02	3.236590E-01	4.179815E-02	-3.458183E-05
3.410445E+03	1.327903E-01	1.079754E-01	-2.481482E-02	8.335700E-03	1.523049E-01	1.951459E-02	4.139953E-05
3.415354E+03	3.513338E-02	1.500150E-02	-2.013186E-02	4.979400E-03	5.439087E-02	1.925748E-02	4.104852E-05
3.420261E+03	-1.111522E-02	-2.432880E-02	-1.321363E-02	2.632400E-03	7.502535E-03	1.861775E-02	4.392363E-05
3.425169E+03	-5.961027E-03	-1.127740E-02	-5.316395E-03	2.073900E-03	5.264774E-03	1.122580E-02	6.856867E-05
3.430077E+03	0.	-9.333200E-03	-9.333193E-03	3.048900E-03	1.680858E-02	1.680858E-02	4.942782E-05
3.434984E+03	-2.131628E-04	-9.481200E-03	-9.481174E-03	3.363200E-03	1.676059E-02	1.676062E-02	4.970553E-05
3.439892E+03	-1.769251E-04	-9.501200E-03	-9.499402E-03	3.756600E-03	1.677510E-02	1.677687E-02	4.993872E-05
3.444800E+03	-4.536815E-05	-9.220600E-03	-9.175242E-03	4.271700E-03	1.669785E-02	1.674322E-02	4.949055E-05
3.449707E+03	-5.586571E-04	-9.005300E-03	-8.446683E-03	5.062300E-03	1.592852E-02	1.648718E-02	5.044775E-05
3.454615E+03	-3.878370E-03	-1.157600E-02	-7.697955E-03	6.062200E-03	1.200883E-02	1.588720E-02	5.224672E-05
3.459523E+03	-1.719712E-02	-2.523090E-02	-8.033766E-03	7.538900E-03	-2.375756E-03	1.482137E-02	5.636149E-05
3.464431E+03	-5.369461E-02	-6.479430E-02	-1.109968E-02	9.224800E-03	-3.981830E-02	1.387630E-02	5.937208E-05
3.469339E+03	-1.274150E-01	-1.446981E-01	-1.728307E-02	1.057760E-02	-1.136846E-01	1.373042E-02	5.989768E-05
3.474247E+03	-2.439253E-01	-2.691008E-01	-2.517556E-02	1.095630E-02	-2.291908E-01	1.473450E-02	5.588763E-05
3.479155E+03	-3.947539E-01	-4.272813E-01	-3.252730E-02	1.003530E-02	-3.783475E-01	1.640644E-02	5.027535E-05
3.484063E+03	-5.601490E-01	-5.978040E-01	-3.765499E-02	7.912900E-03	-5.420081E-01	1.814091E-02	4.379454E-05
3.488972E+03	-7.171498E-01	-7.571699E-01	-4.002009E-02	5.048600E-03	-6.977172E-01	1.943256E-02	4.007151E-05
3.493880E+03	-8.471618E-01	-8.874073E-01	-4.024545E-02	1.975000E-03	-8.271118E-01	2.005005E-02	3.711061E-05
3.498788E+03	-9.396791E-01	-9.739639E-01	-3.928481E-02	-8.483000E-04	-9.195892E-01	2.008995E-02	3.696965E-05
3.503696E+03	-9.922043E-01	-1.030313E+00	-3.810851E-02	-3.149100E-03	-9.724528E-01	1.975145E-02	3.877825E-05
3.508603E+03	-1.008062E+00	-1.045612E+00	-3.755021E-02	-4.828500E-03	-9.888412E-01	1.922042E-02	4.056684E-05
3.513511E+03	-9.937569E-01	-1.031867E+00	-3.811034E-02	-5.899300E-03	-9.751726E-01	1.858424E-02	4.260456E-05
3.518419E+03	-9.568190E-01	-9.969566E-01	-4.013761E-02	-6.466600E-03	-9.387852E-01	1.803383E-02	4.462020E-05
3.523326E+03	-9.044097E-01	-9.484911E-01	-4.408140E-02	-6.623300E-03	-8.868474E-01	1.756231E-02	4.534995E-05
3.528234E+03	-8.426173E-01	-8.930476E-01	-5.043033E-02	-6.456600E-03	-8.254127E-01	1.720460E-02	4.653235E-05
3.533141E+03	-7.762285E-01	-8.368103E-01	-6.058175E-02	-6.180800E-03	-7.592257E-01	1.700278E-02	4.802906E-05
3.538048E+03	-7.087826E-01	-7.933753E-01	-8.459710E-02	-5.754200E-03	-6.919622E-01	1.681595E-02	4.799945E-05
3.542956E+03	-6.427287E-01	-6.389328E-01	3.795943E-03	-5.252300E-03	-6.260343E-01	1.669442E-02	4.816821E-05
3.547863E+03	-5.796891E-01	-5.759056E-01	3.783589E-03	-4.740400E-03	-5.629814E-01	1.670777E-02	4.790572E-05
3.552771E+03	-5.206237E-01	-5.169908E-01	3.632956E-03	-4.238900E-03	-5.039402E-01	1.668349E-02	4.822481E-05
3.557678E+03	-4.660302E-01	-4.626115E-01	3.418714E-03	-3.756300E-03	-4.493736E-01	1.665659E-02	4.869996E-05
3.562586E+03	-4.160616E-01	-4.129212E-01	3.160439E-03	-3.303400E-03	-3.994216E-01	1.666002E-02	4.834261E-05
3.567493E+03	-3.707338E-01	-3.678395E-01	2.894304E-03	-2.854700E-03	-3.540226E-01	1.671116E-02	4.779581E-05
3.572401E+03	-3.298046E-01	-3.271807E-01	2.623865E-03	-2.520900E-03	-3.130907E-01	1.671389E-02	4.837208E-05

TABLE II.- ORIGINAL AND RECONSTRUCTED MODEL FOR ATMOSPHERE AND IONOSPHERE OF MARS – Concluded

		ABEL			HERGLOTZ-WIECHERT		
PLANETOCENTRIC RADIUS (km)	MODEL REFRACTIVITY (N Units)	REFRACTIVITY CALCULATED (N Units)	REFRACTIVITY DIFFERENCE (N Units)	MINIMUM RADIUS DIFFERENCE (km)	REFRACTIVITY CALCULATED (N Units)	REFRACTIVITY DIFFERENCE (N Units)	MINIMUM RADIUS DIFFERENCE (km)
3.577309E+03	-2.930299E-01	-2.906433E-01	2.386626E-03	-2.190900E-03	-2.762963E-01	1.673366E-02	4.760509E-05
3.582216E+03	-2.601030E-01	-2.580032E-01	2.099788E-03	-1.851700E-03	-2.432756E-01	1.682738E-02	4.707280E-05
3.587124E+03	-2.307005E-01	-2.287941E-01	1.906335E-03	-1.629300E-03	-2.137700E-01	1.693051E-02	4.687386E-05
3.592031E+03	-2.045000E-01	-2.028152E-01	1.684812E-03	-1.399700E-03	-1.875528E-01	1.694725E-02	4.682249E-05
3.596939E+03	-1.811908E-01	-1.796952E-01	1.495607E-03	-1.198600E-03	-1.642285E-01	1.696226E-02	4.615721E-05
3.601847E+03	-1.604799E-01	-1.591560E-01	1.323926E-03	-1.032400E-03	-1.435270E-01	1.695292E-02	4.675407E-05
3.606754E+03	-1.420559E-01	-1.409339E-01	1.161927E-03	-8.769000E-04	-1.250687E-01	1.702713E-02	4.610226E-05
3.611662E+03	-1.257696E-01	-1.247573E-01	1.032481E-03	-7.388000E-04	-1.086742E-01	1.711555E-02	4.592599E-05
3.616569E+03	-1.113355E-01	-1.104472E-01	8.883185E-04	-6.248000E-04	-9.412870E-02	1.720678E-02	4.502850E-05
3.621477E+03	-9.852864E-02	-9.776060E-02	7.680520E-04	-5.321000E-04	-8.130462E-02	1.722402E-02	4.548815E-05
3.626385E+03	-8.718565E-02	-8.650690E-02	6.787579E-04	-4.479000E-04	-6.992503E-02	1.726062E-02	4.484699E-05
3.631292E+03	-7.714205E-02	-7.658590E-02	5.561619E-04	-3.702000E-04	-5.979472E-02	1.734733E-02	4.477450E-05
3.636200E+03	-6.825098E-02	-6.780840E-02	4.425436E-04	-3.066000E-04	-5.085020E-02	1.740078E-02	4.392184E-05
3.641108E+03	-6.038158E-02	-6.003390E-02	3.476467E-04	-2.552000E-04	-4.287870E-02	1.750288E-02	4.439140E-05
3.646015E+03	-5.341738E-02	-5.317480E-02	2.425506E-04	-2.046000E-04	-3.585352E-02	1.756386E-02	4.331884E-05
3.650923E+03	-4.725492E-02	-4.720930E-02	4.566511E-05	-1.631000E-04	-2.960644E-02	1.764848E-02	4.307326E-05
3.655831E+03	-4.180237E-02	-4.195710E-02	-1.947614E-04	-1.289000E-04	-2.401956E-02	1.778281E-02	4.302399E-05
3.660738E+03	-3.697826E-02	-3.785090E-02	-8.726705E-04	-9.040000E-05	-1.903069E-02	1.794757E-02	4.218853E-05
3.665646E+03	-3.271037E-02	-3.783140E-02	-5.121046E-03	-5.390000E-05	-1.451050E-02	1.819986E-02	4.102734E-05
3.670554E+03	0.	6.000000E-07	5.752700E-07	3.900001E-06	-1.121518E-02	-1.121518E-02	4.129237E-05
3.675461E+03	0.	7.000000E-07	6.953485E-07	1.599998E-06	-1.098117E-02	-1.098117E-02	4.081859E-05
3.680369E+03	0.	8.000000E-07	8.072145E-07	-7.999915E-07	-1.066110E-02	-1.066110E-02	3.901715E-05
3.685277E+03	0.	2.000000E-07	1.738157E-07	-3.099995E-06	-1.018172E-02	-1.018172E-02	3.759084E-05
3.690185E+03	0.	1.200000E-06	1.158959E-06	4.599991E-06	-9.338130E-03	-9.338130E-03	3.485559E-05
3.695092E+03	0.	0.	0.	2.300003E-06	-6.765603E-03	-6.765603E-03	2.470613E-05

TABLE III.- ORIGINAL AND RECONSTRUCTED MODEL FOR SUN CORONA

[Reconstructed by Abel transform and Herglotz-Wiechert transform]

		ABEL			HERGLOTZ-WIECHERT		
HELIOCENTRIC RADIUS (km)	MODEL REFRACTIVITY (N Units)	REFRACTIVITY CALCULATED (N Units)	REFRACTIVITY DIFFERENCE (N Units)	MINIMUM RADIUS DIFFERENCE (km)	REFRACTIVITY CALCULATED (N Units)	REFRACTIVITY DIFFERENCE (N Units)	MINIMUM RADIUS DIFFERENCE (km)
6.993859E+05	-4.343162E+03	-1.864356E+03	2.478806E+03	-5.847763E+04	-5.261392E+03	-9.182301E+02	6.473435E+02
8.361907E+05	-6.626276E+02	-5.549883E+02	1.276393E+02	-7.293757E+03	-7.473042E+02	-6.467665E+01	5.557484E+01
9.751027E+05	-2.210601E+02	-1.987172E+02	2.234250E+01	-2.051222E+03	-2.322189E+02	-1.115878E+01	1.212716E+01
1.114265E+06	-9.471537E+01	-9.220999E+01	2.505381E+00	-8.251700E+02	-9.754703E+01	-2.831661E+00	4.243751E+00
1.253488E+06	-4.617575E+01	-6.528525E+01	-1.910950E+01	-3.854400E+02	-4.728876E+01	-1.113011E+00	2.361720E+00
1.392734E+06	-2.445677E+01	-2.278606E+01	1.670709E+00	-1.960800E+02	-2.508665E+01	-6.298858E-01	1.747962E+00
1.531991E+06	-1.379007E+01	-1.296253E+01	8.275463E-01	-1.059300E+02	-1.443760E+01	-6.475279E-01	1.783167E+00
1.671249E+06	-8.178486E+00	-7.746205E+00	4.322802E-01	-5.950000E+01	-8.926082E+00	-7.475966E-01	1.974660E+00
1.810519E+06	-5.056566E+00	-4.825074E+00	2.334922E-01	-3.522000E+01	-5.286475E+00	-2.279088E-01	1.082320E+00
1.949786E+06	-3.242594E+00	-3.115485E+00	1.271097E-01	-2.127000E+01	-3.640428E+00	-3.978330E-01	1.397466E+00
2.089048E+06	-2.143430E+00	-2.077125E+00	6.630460E-02	-1.313000E+01	-2.680679E+00	-5.372491E-01	1.702287E+00
2.228323E+06	-1.455206E+00	-1.426932E+00	2.827345E-02	-8.280000E+00	-1.607415E+00	-1.522089E-01	8.835771E-01
2.367592E+06	-1.011459E+00	-1.010961E+00	4.981830E-04	-5.240000E+00	-1.313160E+00	-3.017009E-01	1.226672E+00
2.506854E+06	-7.178163E-01	-7.449766E-01	-2.716022E-02	-3.350000E+00	-1.131507E+00	-4.136904E-01	1.520673E+00
2.646131E+06	-5.189420E-01	-6.259538E-01	-1.070119E-01	-2.190000E+00	-5.695573E-01	-5.061527E-02	5.917476E-01

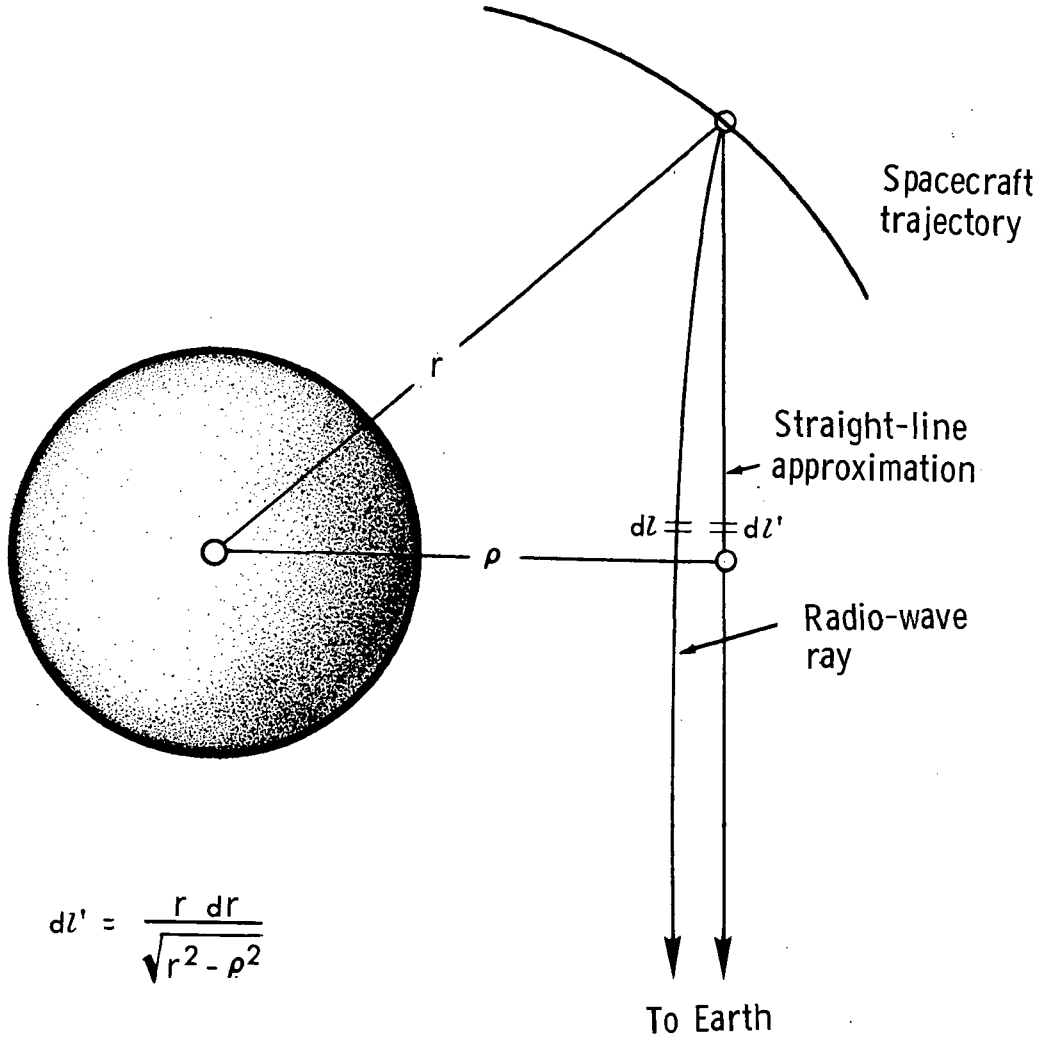

Figure 1.- Abel transform geometry.

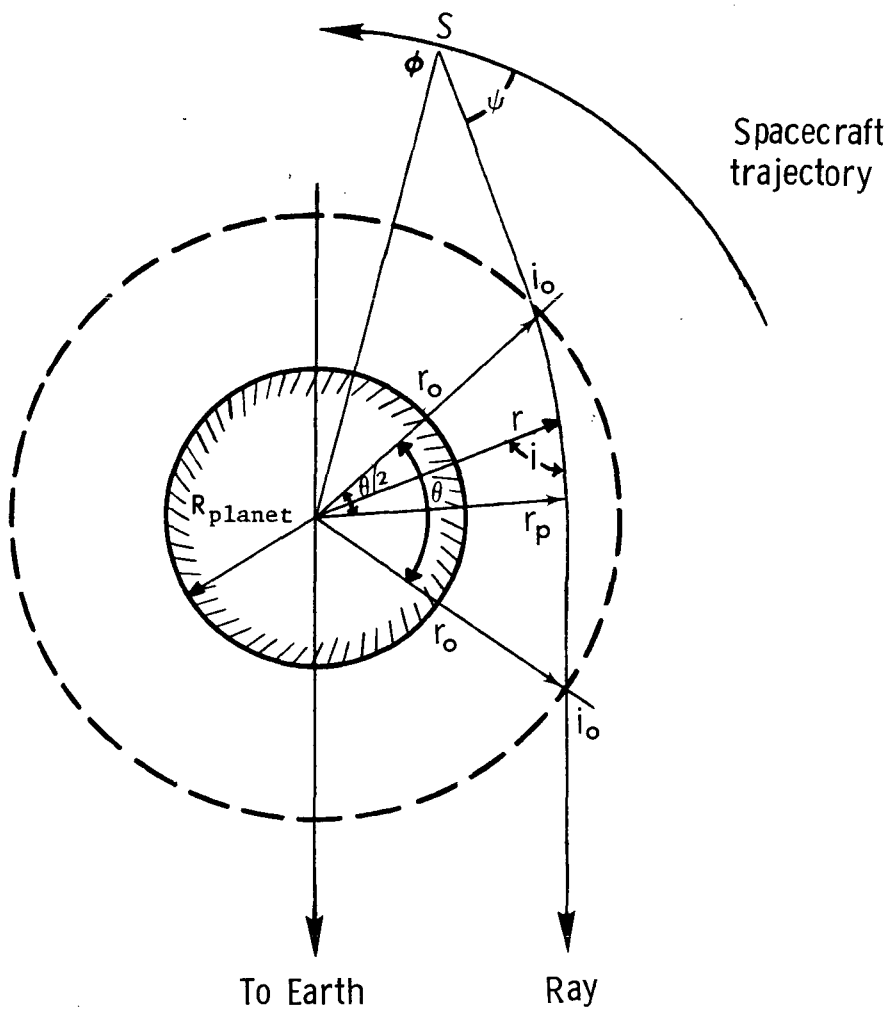

Figure 2.- Seismic transform geometry.

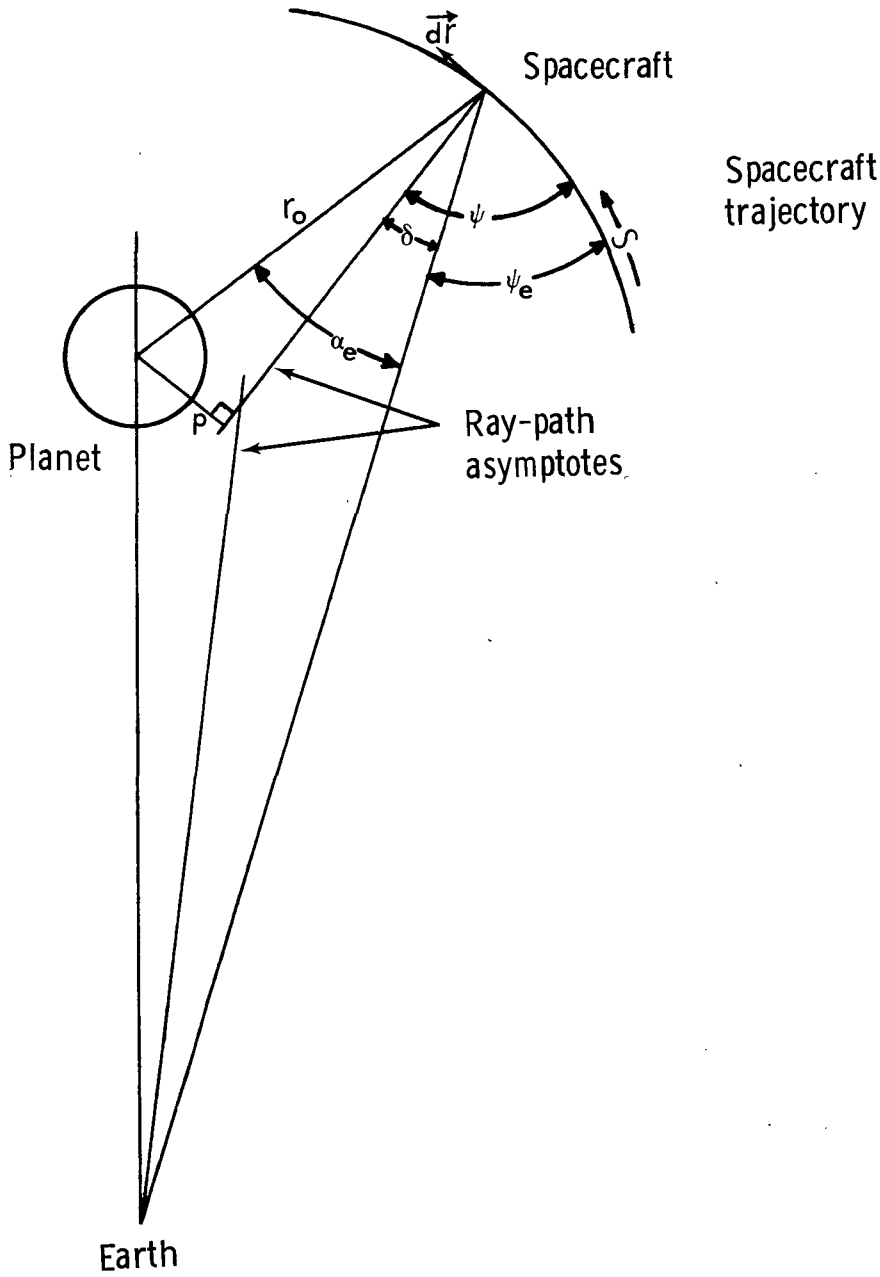

Figure 3.- Impact parameter geometry.

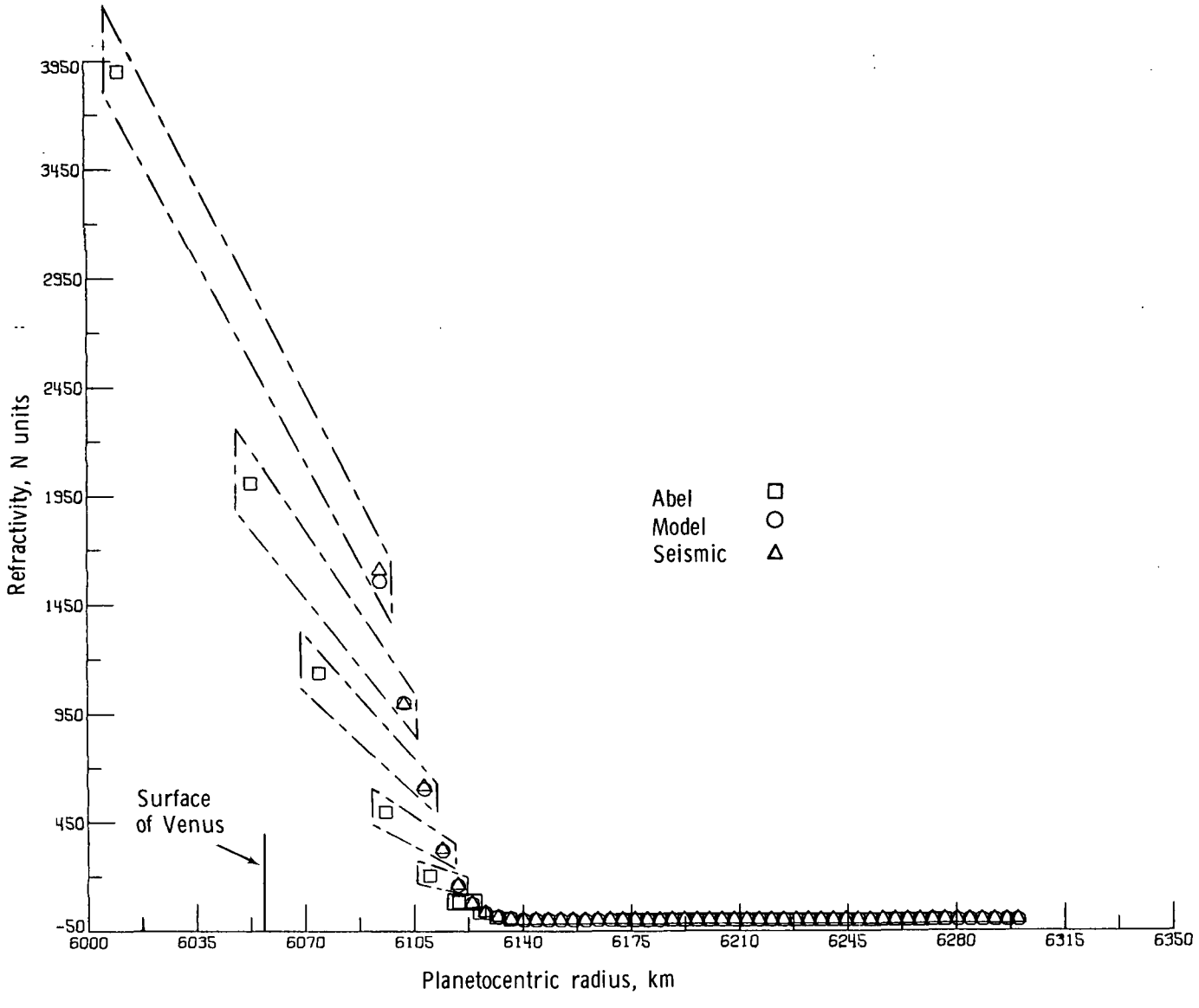

Figure 4.- Model of Venus refractivity profile and its reconstruction by Abel transform and Herglotz-Wiechert transform. (Rectangles traced around the pairs of circles, squares, and triangles identify the original and the reconstructed point.)

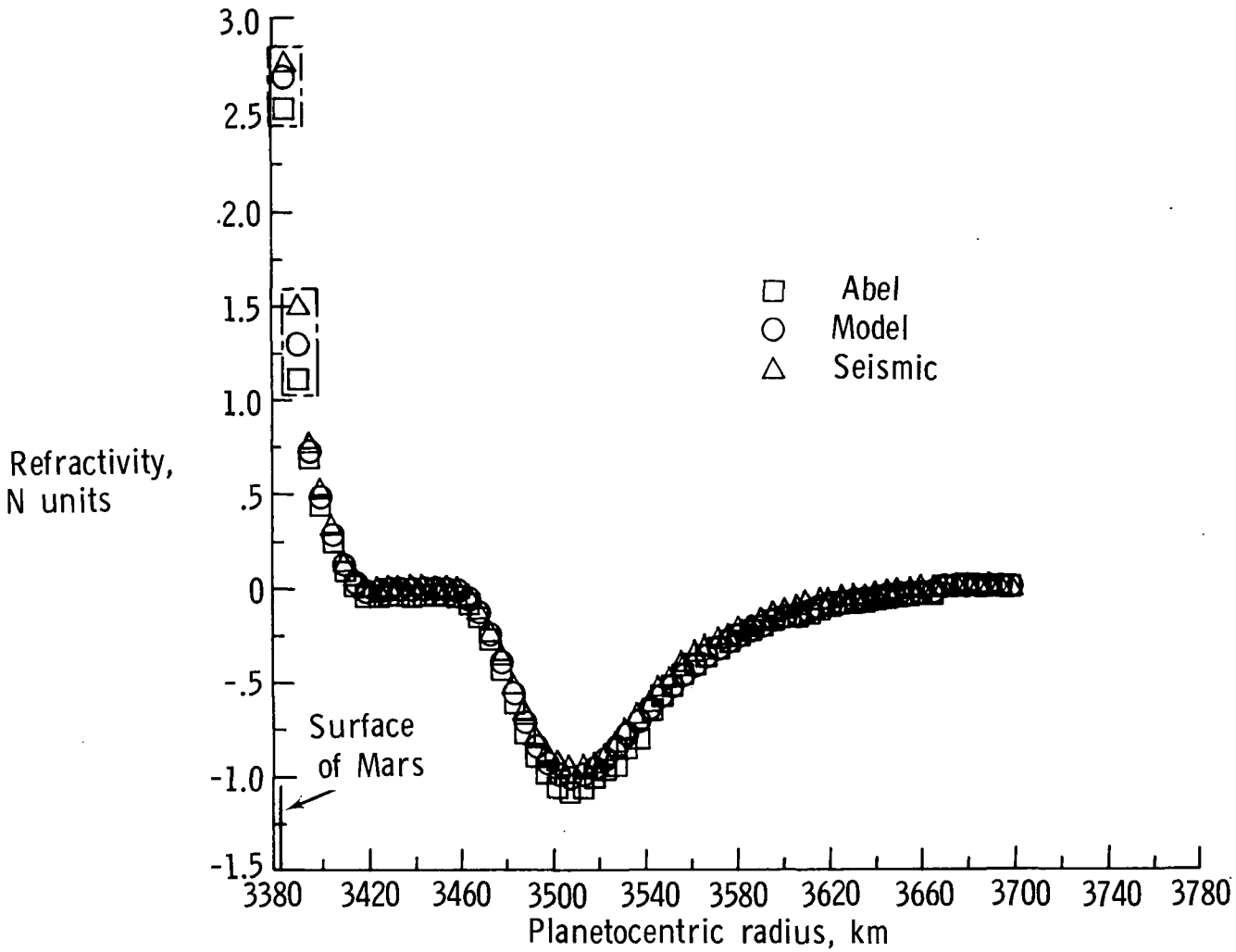

Figure 5.- Model of Mars refractivity profile and its reconstruction by Abel transform and Herglotz-Wiechert transform. (Rectangles traced around the pairs of circles, squares, and triangles identify the original and the reconstructed point.)

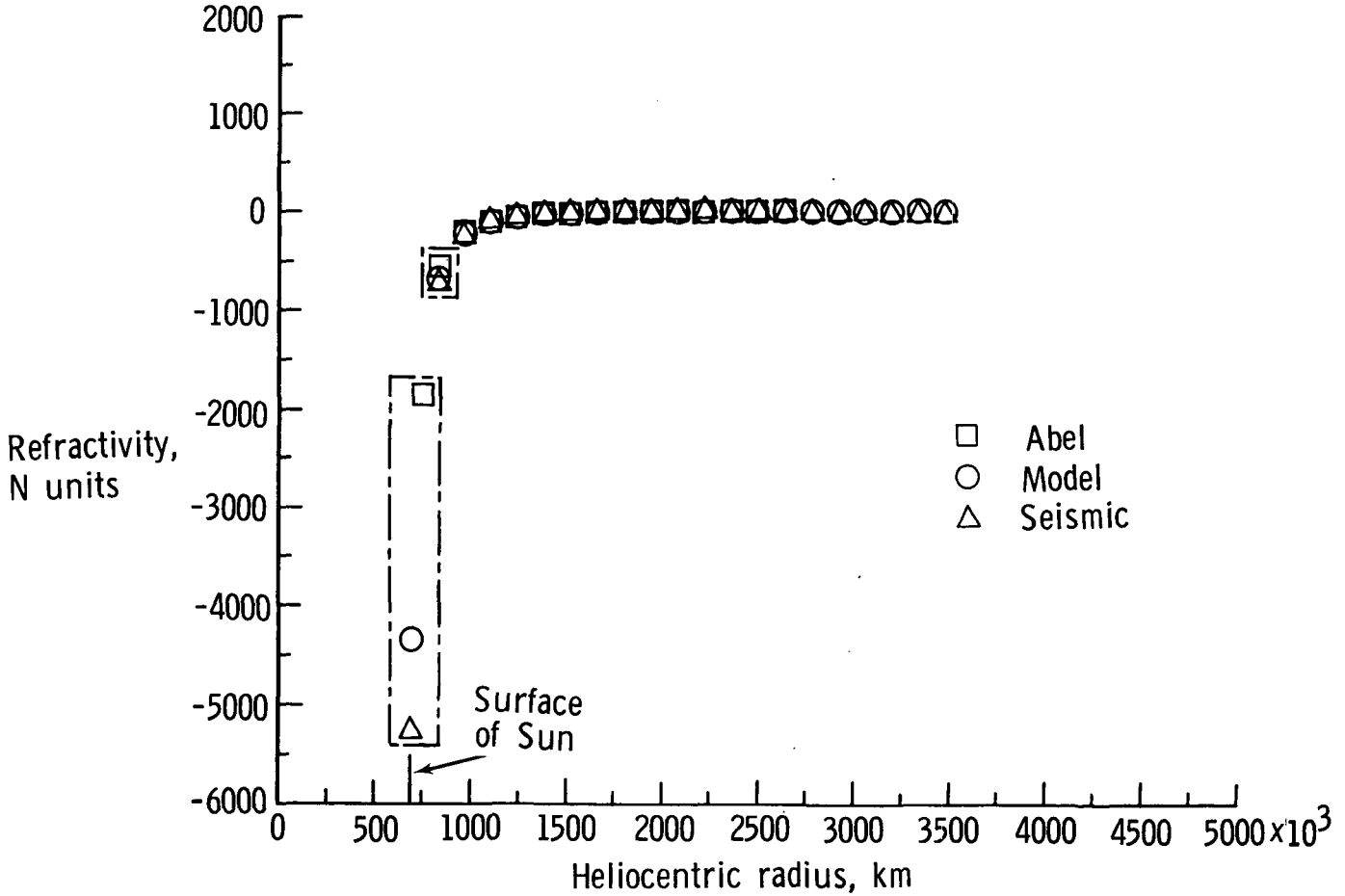

Figure 6.- Model of Sun corona refractivity profile and its reconstruction by Abel transform and Herglotz-Wiechert transform. (Rectangles traced around the pairs of circles, squares, and triangles identify the original and the reconstructed point.)

NATIONAL AERONAUTICS AND SPACE ADMINISTRATION
WASHINGTON, D.C. 20546

OFFICIAL BUSINESS
PENALTY FOR PRIVATE USE $300

SPECIAL FOURTH-CLASS RATE BOOK

POSTAGE AND FEES PAID
NATIONAL AERONAUTICS AND SPACE ADMINISTRATION
451

U.S.MAIL

POSTMASTER: If Undeliverable (Section 158 Postal Manual) Do Not Return

"The aeronautical and space activities of the United States shall be conducted so as to contribute . . . to the expansion of human knowledge of phenomena in the atmosphere and space. The Administration shall provide for the widest practicable and appropriate dissemination of information concerning its activities and the results thereof."

—NATIONAL AERONAUTICS AND SPACE ACT OF 1958

NASA SCIENTIFIC AND TECHNICAL PUBLICATIONS

TECHNICAL REPORTS: Scientific and technical information considered important, complete, and a lasting contribution to existing knowledge.

TECHNICAL NOTES: Information less broad in scope but nevertheless of importance as a contribution to existing knowledge.

TECHNICAL MEMORANDUMS: Information receiving limited distribution because of preliminary data, security classification, or other reasons. Also includes conference proceedings with either limited or unlimited distribution.

CONTRACTOR REPORTS: Scientific and technical information generated under a NASA contract or grant and considered an important contribution to existing knowledge.

TECHNICAL TRANSLATIONS: Information published in a foreign language considered to merit NASA distribution in English.

SPECIAL PUBLICATIONS: Information derived from or of value to NASA activities. Publications include final reports of major projects, monographs, data compilations, handbooks, sourcebooks, and special bibliographies.

TECHNOLOGY UTILIZATION PUBLICATIONS: Information on technology used by NASA that may be of particular interest in commercial and other non-aerospace applications. Publications include Tech Briefs, Technology Utilization Reports and Technology Surveys.

Details on the availability of these publications may be obtained from:

SCIENTIFIC AND TECHNICAL INFORMATION OFFICE

NATIONAL AERONAUTICS AND SPACE ADMINISTRATION

Washington, D.C. 20546